Princeton Plasma Physics Laboratory

PPPL- 5032

PPPL- 5032

Magnetic Diagnostics For Equilibrium Reconstruction And Realtime Plasma Control In NSTX-Upgrade

Stefan Gerhardt, et. al.

JUNE, 2014

PPPL PRINCETON PLASMA PHYSICS LABORATORY

Prepared for the U.S. Department of Energy under Contract DE-AC02-09CH11466.

Princeton Plasma Physics Laboratory
Report Disclaimers

Full Legal Disclaimer

Trademark Disclaimer

PPPL Report Availability

Princeton Plasma Physics Laboratory:

http://www.pppl.gov/techreports.cfm

Office of Scientific and Technical Information (OSTI):

http://www.osti.gov/bridge

Related Links:

U.S. Department of Energy

Office of Scientific and Technical Information

Fusion Links

Magnetic Diagnostics For Equilibrium Reconstruction and Realtime Plasma Control in NSTX-Upgrade[a)]

S.P. Gerhardt,[1] K. Erickson,[1] R. Kaita,[1] J. Lawson,[1] R. Mozulay,[1] D. Mueller,[1] W. Que,[1] N. Rahman,[1] H. Schneider,[1] G. Smalley,[1] K. Tresemer[1]

[1]*Princeton Plasma Physics Laboratory, Princeton, New Jersey 08543, USA*

This paper describes aspects of magnetic diagnostics for realtime control in NSTX-U. The sensor arrangement on the upgraded center column is described. New analog and digital circuitry for processing the plasma current rogowski data are presented. An improved algorithm for estimating the plasma vertical velocity for feedback control is presented

I. THE MANUSCRIPT

Magnetic measurements are critical for the realtime control of the plasma current [1], plasma boundary shape [2,3], plasma position within the vacuum chamber [4-11], plasma beta [12], n≥1 error fields and growing instabilities [13-22], internal profiles [2,23], and disruption proximity [24-32]. This paper describes some aspects of realtime magnetics measurements for NSTX-U [33,34]. Section 2 describes the new magnetic sensors measurements on the center column, while Section 3 describes the new circuitry to process the plasma current signals. Section 4 describes means to estimate the plasma vertical velocity from pairs of flux loop voltages.

II. New Center Column Measurements

The center column for NSTX-Upgrade is significantly larger than on NSTX. This allows a larger number of sensors to be embedded in the plasma facing components. The arrangement of these sensors is shown in Fig. 1a), where the tiles have been "unwrapped". Here, the rows at the top and bottom are the horizontal inner targets, and rows 7-21 correspond to the narrow part of the CS (see Fig. 2).

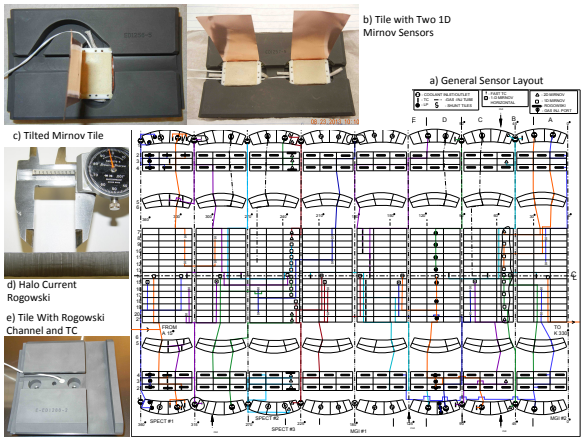

Fig. 1: Layout of sensors on the NSTX-U center column, and photos of sensors imbedded in tiles.

Square symbols represent "1-D Mirnov" sensors, as indicated by the legend in the upper fight of frame a). These 1-D Mirnov sensors are magnetic pickup coils that are wound to measure fields in a single direction. In contrast to NSTX, which had only a single column of these sensors, a second column has been added to NSTX-U at 60° toroidal angle for improved redundancy. An example of two 1D Mirnov sensors imbedded in a single tile is shown in Fig. 1b); the copper sheets are electrostatic shields which will be bent over and then pressed against the Inconel CS casing. The triangles in frame a) represent 2D Mirnov sensors, which have the same physical size as the 1D sensors and are mounted in tiles similar to as shown in Fig. 1b). All of these Mirnov sensors are wounds using bare copper wire onto Macor mandrels; the bare wire provides high-temperature compatibility, and the turns are insulated from each other after winding with Fortafix high temperature cement.

Sensor Type	Sensor Usage	NSTX Count	NSTX-U Count
1D Mirnovs	Fluctuation Analysis, Equilibrium Reconstruction	11	32
2D Mirnovs	Equilibrium Analysis	10	20
Shunt Tiles	Currents Flowing Into the Center Stack	0	18
Tilted Mirnovs	Rod Current, Currents Flowing Vertically in the CS Casing	0	5
Halo Current Rogowskis	Rod Current, Currents Flowing Vertically in the CS Casing	4	4

Table #1: Sensor counts on the center column

There are also rotated 1-D Mirnov sensors, oriented to measure the toroidal field; an example is shown in Fig. 1c). These sensors will be used to assess halo currents on the CS using the same techniques as were used to assess halo currents in the outer divertor in reference [35]. These halo currents are also measured by special rogowski coils oriented in the horizontal plane, so as to measure vertically flowing currents on the center column (and also the TF rod current). An example of this rogowski is shown in Fig. 1d), and Fig. 1e) illustrates the cutout in the back of a tile to contain the path of the rogowski. Note that as in NSTX, the lower halo current rogowski nearest the midplane is segmented into three sections. The final set of sensors for halo current measurements are 18 shunt tiles similar in design to that implemented in the outboard divertor of NSTX and described in Refs. [35,36]. The overall comparison of in-

vacuum sensor counts on the NSTX and NSTX-U center columns is given in Table #1.

There are flux loops and thermocouples mounted on the OH coil, PF-1a coils, PF-1b coils, and on the coil mandrels. Some of these loops are labeled in Fig. 2.

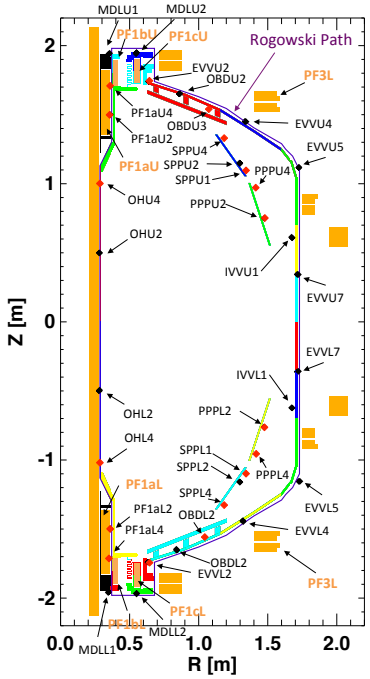

Fig. 2: Layout of flux loops used for vertical position control and plasma current calculation. The red diamonds indicate the 9 loop pairs used in the vertical velocity measurement; these are sometimes additionally used in the I_p calculator system to estimate plate currents. There are many other loops which are used for equilibrium reconstruction (both rtEFIT and offline codes), but are not shown for the sake of simplicity. The different colors represent the different regions of the vessel which are used for the I_P measurement correction. The path of the rogowsk is indicated as well.

III. New Plasma Current Measurements

As part of the CS upgrade, the two plasma current rogowski sensors had to be replaced. As described in Ref. [1], the NSTX rogowskis were located outside the vessel, and linked a single PF coil. Many hundreds of kA of toroidal vessel current were typically recorded during the breakdown phase [1]. For NSTX-U, the rogowski sensors link both the vessel and four total PF coils (the PF-1bU, PF-1cU, PF-1bL, and PF-1cL coils, see Fig. 2). As a consequence, it is possible for the sensor to link up to 4 MA of current, with 2 MA of plasma current and up to 2 MA-turns of divertor coil current. However, it remains desirable to accurately assess currents as low as 5 kA for coaxial helicity injection [37,38] applications. In order to make accurate measurements over this large dynamic range, both high-gain and low-gain plasma current channels will exist on NSTX-U.

The I_P calculator circuit for NSTX-Upgrade has been redesigned to accommodate these machine changes and use modern digital circuitry; see Fig. 3 for a schematic description. Following the method in Ref. 1, the NSTX vessel is divided into multiple sections; these are indicated by the different colors in Fig. 2. The currents in these sections are measured via the equation $I_{ves}=V_{loop}/R_{ves}$, where V_{loop} is the voltage from a flux loop on or near the segment, and R_{ves} is the toroidal resistance of the vessel segment. This calculation of the 24 individual I_{ves} values is done in analog circuits, with a common circuit board designed to output the sum of the currents from four loops, typically with an analog transfer function of 60 kA/V. Six of these 4-channel boards exist, with two of them connected to loops at the potential of the inner vessel and four of them connected to loops on the outer vessel. Note that the NSTX-U vessel is composed of stainless steel inner and outer vessel, with ceramic breaks at the top and bottom to provide insulation. This design facilitates CHI experiments. These six signals plus the four signals from the two rogowskis are fiber-optically coupled to a digital processing circuit in a remote electronics room.

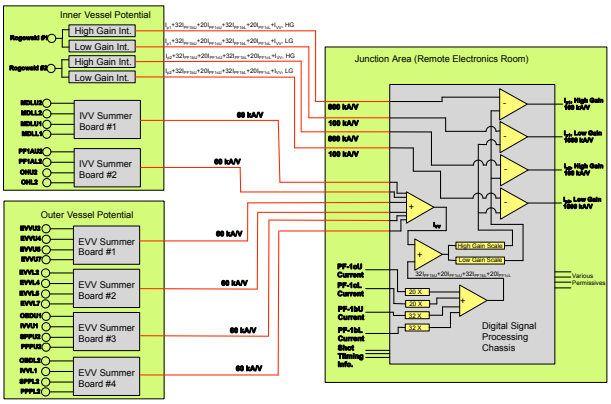

Fig. 3: Schematic of the I_P calculator for NSTX-Upgrade

The digital processing circuitry in the remote electronics room has access to these 10 signals, the currents in the linked coils, and the various NSTX-U timing signals. Calibration factors for the inputs can be applied and easily adjusted. The digital electronics evaluate four instances of the equation $I_P = I_{Rog} - 32I_{PF1bU} - 32I_{PF1bL} - 20I_{PF1cU} - 20I_{PF1cL} - I_{VV}$, where the four instances correspond to the high and low gain signals from rogowskis 1 and 2. The term I_{VV} is the signal resulting from the sum of the six vessel current summations.

The I_P calculator chassis also provides addition outputs. An interlock for the neutral beams is provided based on a minimum I_P threshold; this prevents the neutral beams from injecting into the torus for >50 ms in the absence of a plasma. Interlocks are also provided to the RF heating and gas delivery control systems.

IV. Improved Estimates of the Plasma Vertical Position

Vertical position control is a requirement for all elongated tokamaks, and becomes increasingly challenging as the aspect ratio is increased, due to the reduction in the natural elongation [39,40]. While NSTX seldom had trouble with vertical stability during the quiescent flat-top of the discharge, there is evidence that vertical control will be more difficult in the larger aspect ratio NSTX-Upgrade [41]. Hence, an effort has been made to develop improved vertical control, including improved detection of vertical motion as described here.

In NSTX, the voltage on the radial field coils has a term proportional to the quantity V_{PPPU2}-V_{PPPL2} [3]; this quantity is added to the PF3U voltage request and subtracted from the PF3L voltage request. Note that the measured voltage difference is between otherwise identical loops located above and below the

midplane, on the outboard side. The correct selection of the loops for sensing vertical motion of the plasma has been discussed in the literature [4,5,7,10] In order to assess if inclusion of additional loops in the NSTX controller will help with control, it is assumed that the quantity $I_P Z_P$ can be expressed as a sum of flux differences

$$I_P Z_P = \sum_i \alpha_i (\psi_{U,i} - \psi_{L,i}), \quad (1)$$

where i is a loop over pairs of flux loops. This reduces to the present controller if α_{PPP2} is finite and all other values of α are zero. For constant I_P, the difference in flux loop voltages is thus proportional to dZ_P/dt.

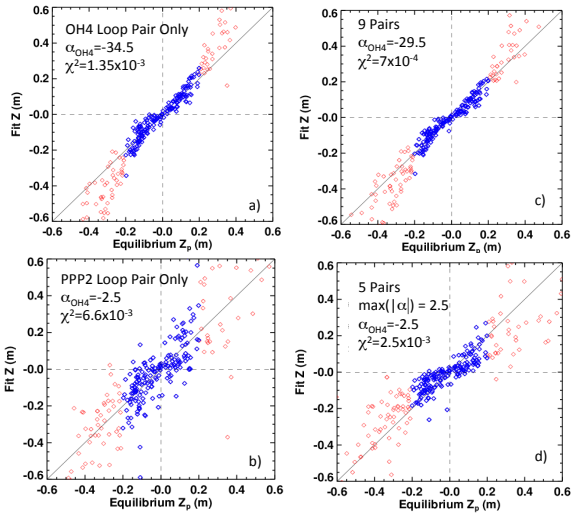

Fig. 4: Various fits with Eqn. 1. See text for details.

In order to determine the optimal values of α for a set of up to 9 loop-pairs distributed around the vessel, a large database of equilibria was formed. These include many cases from EFIT [42,43] reconstructions that explicitly include realistic vessel currents. Only cases with $|Z_P|$<0.2 m are included in the present analysis, as larger plasma displacements are likely not controllable. This results in 172 different equilibria to be included in the fitting process. The presentation here considers NSTX equilibria only; NSTX-U equilibria will replace these once experimental equilibria with realistic eddy currents are available with the initiation of experimental operations.

When equation (1) is fit to the database allowing only the OH4 loops pair(top and bottom of the OH coil within the CS), an excellent fit is found with $\alpha_{PH4} = -34.5$, as shown in Fig. 4a). On the other hand, when the fit is done allowing only the PPP2 loop pair (those in the previously implemented controller), the fit is far less accurate as captured by the χ^2 parameter in Fig 4b), and has a much lower weight coefficient of $\alpha_{PPP2} = -2.5$.

This fitting process was done using a set of 9 loop pairs, in order to determine whether this would result in substantially better fits than cases with only single loop pairs. The results in Fig. 4c) show that the fit is approximately a factor of two better compared to the case in Fig. 4a). The optimizer still places the dominant weight on the OH4 loop pair, located on the center column.

A final test was made where there was a maximum weight allowed for any give loop pair, in an attempt to force a more even weighting amongst the various sensors. The results from this are shown in Fig. 4d). Once the value of the maximum allowed |α| is reduced below ~30, the optimizer always places the maximum allowed value on the OH4 loops. For instance, in frame d), the maximum allowed |α| is 2.5, and the optimizer does indeed set α_{OH4}=-2.5. Even in this case, the fit is 6.6/2.5 = 2.5 times better then using the PPP2 loops alone.

A key experimental question outside of the present analysis is to determine which loop pairs are most insensitive to n=1 perturbations in the plasma; this sensitivity would be due to tilts in the loop orientation and pickup in the leads. This will be analyzed when NSTX-U begins operations, and those loops with minimal n=1 sensitivity selected for improved position control.

Acknowledgements
This research was funded by the United States Department of Energy (DoE) under contract DE-AC02-09CH11466.

References

[1] D. Gates, et al., Rev. Sci. Instrum **75**, 5090 (2004)
[2] J.R. Ferron, et al., Nuclear Fusion **38**, 1055 (1998).
[3] D.A. Gates, et al., Nuclear Fusion **46**, 17 (2006).
[4] N. Pomphrey, et al., Nuclear Fusion **29**, 465(1989)
[5] R. Albanese, et al., Nuclear Fusion **29**, 1013 (1989)
[6] E. A. Lazarus, et al., Phys. Fluids **3**, 2220 (1991).
[7] D.J. Ward and F. Hofmann **34**, 401 (1994).
[8] F. Hofmann, et al., Nuclear Fusion **37**, 681 (1997).
[9] F. Hofmann, et al., Nuclear Fusion **40**, 767 (2000).
[10] C. Kessel, et al., Nuclear Fusion **41**, 953 (2001)
[11] D.A. Humphreys, et al., Nuclear Fusion **49**, 115003 (2009).
[12] S.P. Gerhardt, et al., Fusion Sci. and Tech. **61**, 11 (2012).
[13] A. M. Garofalo, et al., Nuclear Fusion **42**, 1335 (2002).
[14] E. J. Strait, et al., Phys. Plasmas **11**, 2505 (2004).
[15] M. Okabayashi, et al., Nuclear Fusion **45**, 1715 (2005).
[16] S.A. Sabbagh, et al., Phys. Rev. Lett. 97, 045004 (2006).
[17] S.A. Sabbagh, et al., Nuclear Fusion **46**, 635 (2006).
[18] A.M. Garofalo, et al., Nuclear Fusion **47**, 1121 (2007).
[19] M. Okabayashi et al., Nuclear Fusion **49** 125003 (2009)
[20] S.A Sabbagh, et al., Nuclear Fusion **50** (2010) 025020.
[21] J.E. Menard, et al., Nuclear Fusion **50**, 045008 (2010)
[22] S.P. Gerhardt, et al., Nuclear Fusion **53**, 043020 (2013).
[23] D. Moreau et al Nuclear Fusion **51,** 063009 (2011)
[24] Pautasso G. et al 2002 Nuclear Fusion 42 100 (2002)
[25] Yoshino R. et al., Nuclear Fusion 43 1771 (2003)
[26] Cannas B. et al., Nuclear Fusion 44 68 (2004)
[27] Yoshino R. Nuclear Fusion 45 1232 (2005)
[28] Windsor C.G. et al., Nuclear Fusion 45 337 (2005)
[29] Cannas B. et al., Nuclear Fusion 47 1559 (2007)
[30] P.C. DeVries, et al, Nuclear Fusion **49**, 055011 (2009]
[31] Cannas B. et al., Nuclear Fusion 50 075004 (2010)
[32] S.P. Gerhardt, et al., Nuclear Fusion **53**, 063021 (2013).
[33] J.E. Menard et al. Nuclear Fusion **52** 083015 (2012)
[34] S.P. Gerhardt et al Nuclear Fusion **52** 083020 (2011)
[35] S.P. Gerhardt, et al., Rev. Sci. Instrum. **82** , 103502 (2011)
[36] S.P. Gerhardt, Nuclear Fusion **53**, 023005 (2013).
[37] R. Raman, et al., Nuclear Fusion **45** L15 (2005)
[38] R. Raman, et al., Nuclear Fusion **49** 065006 (2009).
[39] M. Roberto, Nuclear Fusion **32**, 1666 (1992).
[40] J.E. Menard, et al., Nuclear Fusion **37**, 595 (1997)
[41] S.P. Gerhardt et al., Nuclear Fusion **51** 073031 (2011)
[42] L. L. Lao, Nuclear Fusion **25**, 1611 (1985).
[43] S.A. Sabbagh, et al., Nuclear Fusion 41, 1601 (2001).

The Princeton Plasma Physics Laboratory is operated
by Princeton University under contract
with the U.S. Department of Energy.

Information Services
Princeton Plasma Physics Laboratory
P.O. Box 451
Princeton, NJ 08543

Phone: 609-243-2245
Fax: 609-243-2751
e-mail: pppl_info@pppl.gov
Internet Address: http://www.pppl.gov